Journal of Photochemistry & Photobiology, A: Chemistry 469 (2025) 116585

Contents lists available at ScienceDirect

Journal of Photochemistry & Photobiology, A: Chemistry

journal homepage: www.elsevier.com/locate/jphotochem

Visible-light photocatalytic activity of a green niobium pentoxide nanocatalyst: Experimental analysis and machine learning approach

Hanna Abdalrahman Mahmud [a], Leandro Rodrigues Oviedo [a], Maurício Dalla Costa Rodrigues da Silva [a,b], Cristiane dos Santos [a], Giovani Pavoski [c], Jorge Alberto Soares Tenório [c], Denise Crocce Romano Espinosa [c], William Leonardo da Silva [a,*]

[a] Applied Nanomaterials Research Group (GPNAp), Nanoscience Graduate Program, Franciscan University (UFN), Santa Maria, RS, Brazil
[b] Federal University of Health Sciences of Porto Alegre (UFCSPA), Porto Alegre, RS, Brazil
[c] Polytechnical School of Chemical Engineering, University of the Sao Paulo, São Paulo, SP, Brazil

ARTICLE INFO

Keywords:
Green nanocatalysts
Niobium pentoxide nanoparticles
Machine learning
Advanced oxidation processes
Decision tree

ABSTRACT

This work aims to develop green Nb_2O_5-NPs from *Carya illinoinensis* extract for the photodegradation of six organic dyes and to predict the reaction degradation progress through a machine learning study. 71.5 % removal was the highest value achieved for dye degradation after 120 min under visible radiation with the apparent rate of the pseudo first-order reaction $k = 0.0034\ min^{-1}$. DT algorithm showed satisfactory performance ($R^2_{training} = 0.9975$ / $R^2_{test} = 0.9945$, $RMSE_{training} = 0.059$ / $RMSE_{test} = 0.094$), predicting 75 % of MB dye removal after 300 min under visible radiation. Nb_2O_5-NPs showed high phytotoxicity for *Beta vulgaris* L. seeds (except at 50 mg L^{-1}) and no phytotoxicity for *Brassica oleracea* seeds in all concentrations tested (12.5–100 mg L^{-1}). Therefore, this study highlights the importance of integrating machine learning models into catalytic research, offering valuable insights for optimizing reaction conditions and guiding scalable photodegradation processes.

1. Introduction

In recent years, issues related to sustainability and environmental impacts have generated global repercussions. One of the biggest environmental challenges concerns the incorrect disposal of enormous quantities of organic compounds, especially synthetic dyes, in ecosystems, such as water bodies [1]. These dyes are responsible for a series of problems for fauna and flora, mainly due to their carcinogenic potential, affecting the photosynthesis process [2].

It is estimated that approximately 700,000 tons of synthetic dyes are produced annually by the textile industry [3]. These dyes, in addition to being toxic to the environment, cause skin and eye irritation in humans [4]. Thus, there is a constant search for advances that improve the methods of treating these compounds in the water environment, with the aim of improving conventional processes, such as physical-chemical and biological treatments [5]. However, these processes have limitations, especially in the removal of certain substances, such as synthetic dyes present in wastewater, which reduces their effectiveness [6].

A promising alternative for wastewater treatment is advanced oxidation processes (AOPs) [7].These processes are effective in degrading synthetic organic dye molecules, ensuring a high removal rate and the possibility of using alternative nanomaterials, such as photocatalysts, with emphasis on heterogeneous photocatalysis [8].

Nanotechnology has been widely explored as a solution to these environmental challenges and processes such as photocatalysis [9]. Nanocatalysts (*e.g.*, zinc oxide nanoparticles / ZnO-NPs, niobium pentoxide nanoparticles / Nb_2O_5-NPs, vanadium pentoxide nanoparticles / V_2O_5-NPs, and titanium dioxide nanoparticles / TiO_2-NPs) are being investigated due to their unique properties and potential in pollutant degradation. In the case of Nb_2O_5-NPs, its remarkable properties, combined with the feasibility of green synthesis, make it a promising material for the treatment of wastewater containing synthetic dyes [8]. Niobium(V) oxide nanoparticles (Nb_2O_5-NPs) stand out for their chemical and thermal stability, in addition to a band gap energy (E_g) ranging from 3.1 to 3.4 eV, as well as porosity, and surface area [10,11].

Green synthesis is an alternative and more sustainable method for the production of nanoparticles, using less toxic and hazardous substances [12]. In the state of Rio Grande do Sul, for example, there is a significant production of pecan nutshell (*Carya illinoinensis*), whose shells are rich in bioactive compounds that can act as reducers and

* Corresponding author.
E-mail address: w.silva@ufn.edu.br (W.L. da Silva).

https://doi.org/10.1016/j.jphotochem.2025.116585
Received 7 February 2025; Received in revised form 9 June 2025; Accepted 17 June 2025
Available online 18 June 2025

Table 1
Technical details of ML algorithms.

Algorithm	Algorithm parameters	Equations	Reference
Decision tree (DT)	Tree maximum depth*: 5, 10, 15, 20, 25 m Number of splits per tree: 5, 10, 12, 15 Performance measured by minimizing the mean squared error R*(T)*, according to Eq. (10)	$R(T) = \frac{1}{N}\sum_{t \epsilon T}\sum_{t \epsilon T}(y_i - \hat{y}_i)^2$ (3) Where: *R(T)* = expected value of the sum of mean squared errors using a constant as a predictive model; *N* is the number of nodes used in the decision/pattern recognition in the data (one node is equivalent to one leaf of the decision tree); y_i = observed value obtained experimentally; $\hat{y}_i$ = predicted value obtained from the model; t = identifier of each node, T = mean squared error between the observed and the predicted values (response).	[19]
Random Forest (RF)	Tree maximum depth: 5, 10, 15, 20, 25 m. Number of decision trees tested: 25, 50, 75, 100 Performance measured by minimizing the mean squared error R*(T)*, as defined in DT algorithm	$R_1(T) = \frac{1}{N}\sum_{t \epsilon T}\sum_{t \epsilon T}\left(y_{i,1} - \widehat{y_{i,1}}\right)^2$ (4) $R_2(T) = \frac{1}{N}\sum_{t \epsilon T}\sum_{t \epsilon T}\left(y_{i,2} - \widehat{y_{i,2}}\right)^2$ (5) $R_{avg}(T) = \frac{R_1(T) + R_2(T)}{2}$ (6) Where: $R_1(T)$ and $R_2(T)$ are the measurements of the performance of groups 1 and 2 of k-decision trees; $R_{avg}(T)$ is the final response of the RF algorithm (average of the decisions of the n–groups made up of k–trees)	
Xtreme gradient boosting (XGBoost)	Tree maximum depth: 1, 2, 3, 4, 5 Number of decision trees tested: 20, 30, 50, 70, 90, 100 Learning rate: 1 %, 2 %, and 3 % Method used to prevent overfitting: L2 regularization with λ = 0.21* Subsamples: 85 % of the dataset Performance is measured by minimizing the mean squared error $R_{avg}(T)$, similar to RF	Similar to RF. This algorithms use optimization functions that guarantee greater computational power, fast convergence to the optimal value predicted by the algorithm, and less probability of overfitting Response = average of the decisions of the n–groups made up of k-trees	
Recurrent neural network with Long short-term memory (RNN-LSTM)	Neural network structure: *m*:*n*:*k*, where *m* is the number of input data (independent variables), *n* is the number of neurons in the hidden layer, which is responsible for processing the data Main node function: Summation/activation function used in each node (Eq. 7), associated with reLu (Eq. 8), logistic (Eq. 9) and hyperbolic tangent (Eq. 10) functions Weight optimization function: Lbfgs, Adam**	$\varphi = \sum w_n \bullet x_n + b_k$ (7) $f(\varphi) = (0, x_{máx})$ (8) $f(\varphi) = \frac{1}{1 - e^{-\varphi}}$ (9) $f(\varphi) = \frac{2}{1 + e^{-2\varphi}} - 1$ (10) Where: φ = transfer function; x_n = n-th neural network node; w_i = weight associated with the nth neuron x_n; b_k = bias (error associated with the prediction model); x = maximum value predicted by the ANN algorithm, using the ReLu function	

cv = 5 for all algorithms tested | * This value represents 21 % of the relative weight assigned to the penalization, aiming to balance model complexity and generalization capability.

stabilizers in the green synthesis of nanoparticles [13]. The reuse of these shells offers an alternative to improper disposal, which often contributes to soil and water pollution.

In this context, the present work aims to synthesize and characterize a green nanocatalyst of niobium(V) oxide nanoparticles (Nb_2O_5-NPs) from *C. illinoinensis* extract for the photodegradation of six organic dyes (methylene blue – MB, gentian violet - GV, rhodamine 6G – Rh6G, rhodamine B – RhB, bromocresol green – BG and bromophenol blue – BB) by heterogeneous photocatalysis under visible radiation and to predict the reaction progress (from 0 to 300 min) for the MB dye degradation with the highest removal through the application of machine learning models. Thus, the novelty of this study is that it relates nanobiotechnology to the Sustainable Development Goals, focusing on ensuring the availability and sustainable management of water and sanitation for all, by developing a sustainable alternative nanomaterial with potential application in wastewater treatment correlating with artificial intelligence through the machine learning tool.

2. Material and methods

2.1. Materials

Pecan nutshell (*C. illinoinensis*) was provided by a pecan nut processing industry in the southern region of Brazil. Niobium(V) chloride ($NbCl_5$, Merck, ACS reagent, 99 %) and ammonium hydroxide (NH_4OH, Synth, ACS reagent, 270 % NH_3 basis 27 %) were used in the Nb_2O_5-NPs biosynthesis. MB ($C_{37}H_{27}N_3Na_2O_9S_3$, Vetec, ACS reagent, powder, ≥ 99 % purity), GV ($C_{25}H_{30}N_3Cl$, Vetec, ACS reagent, powder, ≥ 90 % purity anhydrous basis), Rh6G ($C_{28}H_{31}N_2O_3Cl$, Vetec, ACS reagent, powder, ≥ 99 % purity), RhB ($C_{28}H_{31}ClN_2O_3$, Vetec, ACS reagent, powder, ≥ 95 % purity), BG ($C_{21}H_{14}Br_4O_5S$, Vetec, ACS reagent, powder, ≥ 95 % purity) and BB ($C_{19}H_{10}Br_4O_5S$, Vetec, ACS reagent, powder, ≥ 95 % purity) were the dyes used as target pollutants in the heterogeneous photocatalysis tests.

Isopropyl alcohol ($(CH_3)_2CHOH$, Merck, ACS reagent, ≥99.5 %), potassium dichromate ($K_2Cr_2O_7$, Merck, ACS reagent, ≥99.0 %), L-ascorbic acid ($C_6H_8O_6$, Merck, reagent grade, crystalline) and Ethylenediaminetetraacetic acid (EDTA) ($(HO_2CCH_2)_2NCH_2CH_2N(CH_2CO_2H)_2$, Merck, ACS reagent, 99.4–100.6 %) were used to elucidate the scavenger effect on heterogeneous photocatalysis.

2.2. Preparation of the C. illinoinensis extract

C. illinoinensis extract was prepared by infusion method [14], where 10 g of pecan nutshells were mixed with 500 mL of distilled water under magnetic stirring. Subsequently, the solution was vacuum-filtered (Qualy, 90 mm circle) and stored in an amber flask at 25 ± 2 °C.

2.3. Green synthesis and characterization of Nb_2O_5-NPs

The green synthesis [15] was used for the development of nanoparticles, where *C. illinoinensis* extract (50 mL) was mixed with 50 mL of metal precursor solution (0.1 mol L^{-1} $NbCl_5$) and 5 mL of NH_4OH under magnetic stirring (300 rpm for 60 min) for reduction and nucleation steps. After, the nanomaterial was dried (75 ± 2 °C for 12 h), and calcinated (500 °C for 3 h with 5 °C min^{-1}) to stabilize the nanoparticles.

Nb_2O_5-NPs were characterized by X-Ray Diffraction (XRD), Zeta Potential (ZP), 11-points assay for zero charge point evaluation (pH_{ZCP}), Diffuse Reflectance Spectroscopy (DRS), Scanning Electron Microscopy (SEM), and N_2 porosimetry. More information about characterization is provided in the Supplementary Information (SI).

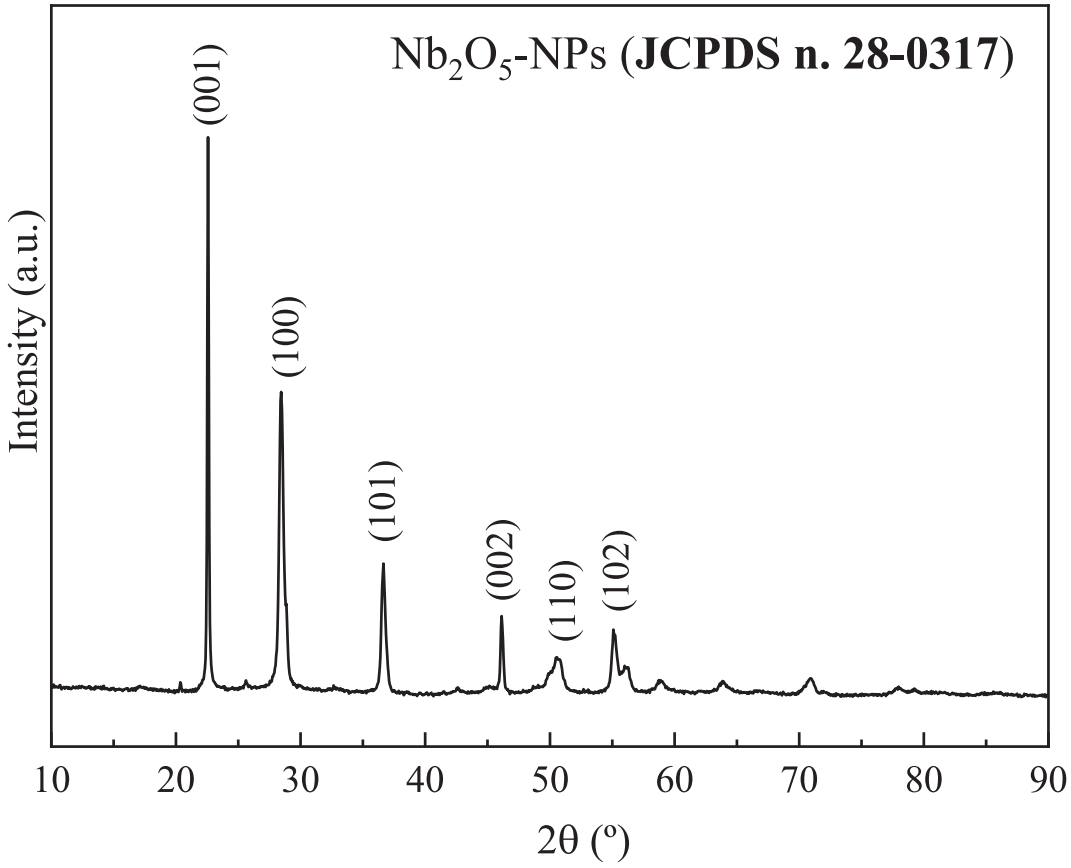

Fig. 1. XRD diffractogram of the Nb_2O_5-NPs from *C. illinoinensis* extract.

2.4. Heterogeneous photocatalysis assay

The photocatalytic tests were carried out in batch mode using six organic dyes (MB, GV, Rh6G, RhB, BG and BB) at concentration of 50 mg L^{-1}, $T = 25 \pm 2$ °C, pH 7, and nanocatalyst (1 g L^{-1}) in a slurry reactor under visible irradiation (LED Bulb with 50 W) in two stages: (a) in dark conditions: adsorption of the dye molecules on the catalytic surface without irradiation (60 min), and (b) photocatalytic degradation of the dyes: under visible radiation, aliquots (~3 mL) were collected at times 0, 15, 30, 45, 60, 75, 90, 105, and 120 min, centrifuged (4500 rpm, 5 min), and diluted (1:10 v v^{-1}). The organic dye concentration was determined by UV–Vis spectrophotometry at 582, 668, 527, 543, 615, and 588 nm for GV, MB, Rh 6G, RhB, BG, BB, respectively (Shimadzu, UV–Vis Mini 1240) [16]. The experimental data were fitted according to the Langmuir-Hinshelwood model method according to Eqs. (1) and (2) [17].

$$(-r_i) = -\frac{dC_i}{dt} = \frac{k_s * K * C_i}{1 + K * C_i} \quad (1)$$

$$C_i = C_{i0} * e^{-k*t} \quad (2)$$

where: $(-r_i)$ is the reaction rate (mol L^{-1} min^{-1}), K is the adsorption coefficient of the compound to be degraded (L mg^{-1}), k_s is the apparent constant of reaction (mol L^{-1} min^{-1}), C_{i0} is the initial dye concentration (mg L^{-1}), C_i is dye concentration at time t (mg L^{-1}), t is the illumination time (min) and *k* is the apparent rate of the pseudo first-order reaction (min^{-1}).

2.5. Reuse of the nanocatalyst

The reuse of the Nb_2O_5-NPs was performed to evaluate the photocatalytic activity after 5 cycles of photodegradation under visible irritation. Moreover, after the first cycle (120 min of irradiation), dye-containing aqueous solutions were centrifuged at 4500 rpm for 5 min to separate the nanocatalysts from the aqueous solution for reuse. Thus, solid nanomaterial was carefully separated and reintroduced in the reactor. Moreover, photocatalytic activity was measured at the end of each cycle.

2.6. Scavenger effect on heterogeneous photocatalysis

To investigate the participation of reactive oxygen species (ROS) and electron-hole pairs in dye degradation reaction, the use of scavengers in heterogeneous photocatalysis was investigated. Thus, 7.65 μL of isopropyl alcohol ($HO^{\bullet}$ scavenger), 29.4 mg of potassium dichromate (e^- scavenger), 17.6 mg of ascorbic acid ($O_2^{-}\bullet$ scavenger), and 29.2 mg of EDTA (h^+ scavenger) were employed to elucidate the photodegradation mechanism [18]. The inhibition/reduction of the degradation efficiency in the presence of these scavengers provides insight into the roles of hydroxyl radicals ($HO^{\bullet}$), superoxide radicals ($O_2^{\bullet}$) photogenerated electrons (e^-), and holes (h^+). This approach enables a deeper understanding of the photocatalytic pathways and the contribution of each reactive species to the overall degradation process.

2.7. Machine learning study

Four ML algorithms were used to predict the degradation reaction progress (from 0 to 300 min) for under visible radiation for the dye molecule with the highest removal in the photocatalytic assay. A detailed description of the algorithms is provided in Table 1. A k-fold cross-validation with cv = 5 was applied to all algorithm configurations, with the algorithms being coded in Python 3.4. Thus, numpy, pandas, sklearn, and seaborn libraries were used for data preprocessing,

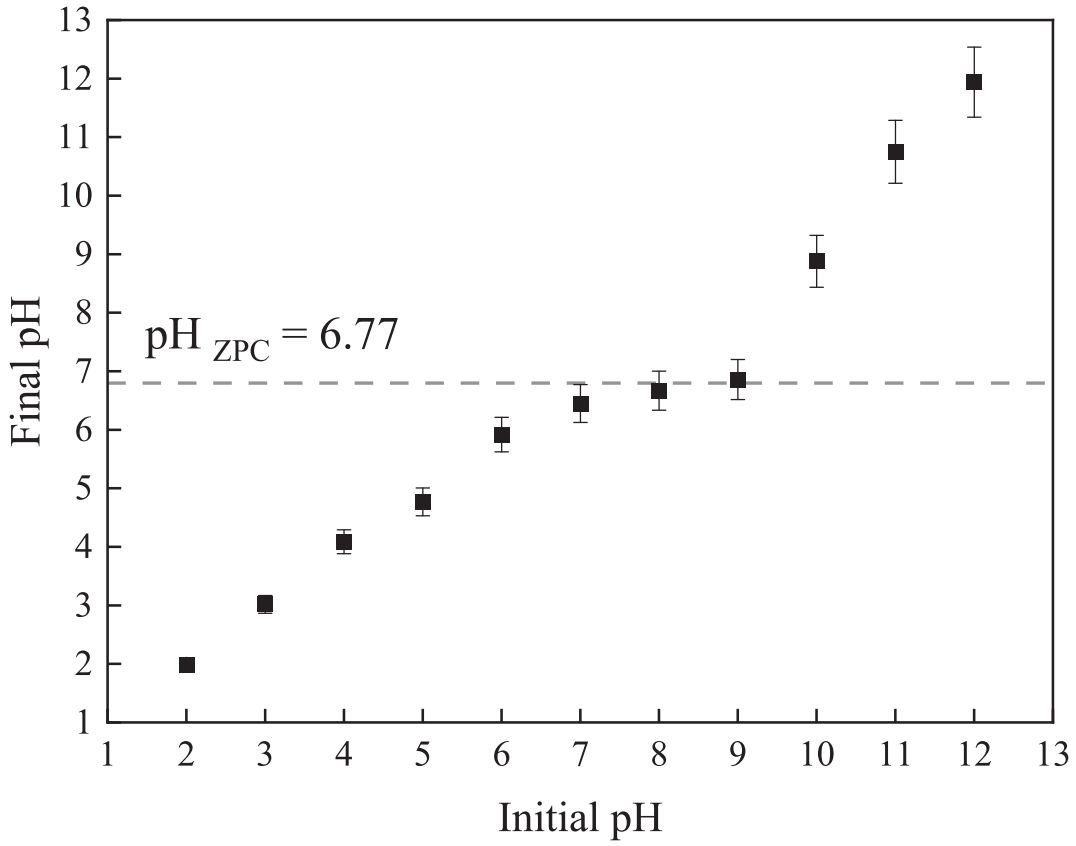

Fig. 2. Zero charge point (pH_{ZCP}) of the Nb_2O_5-NPs from *C. illinoinensis* extract.

Table 2
Textural and surface properties of Nb_2O_5-NPs from *C. illinoinensis* extract.

S_{BET} ($m^2\ g^{-1}$)	V_p ($cm^3\ g^{-1}$)	D_p (nm)	ZP (mV)
171 ± 0.40	0.3 ± 0.01	9.7 ± 0.61	−28.2 ± 0,9

manipulation, machine learning algorithm compilation and metrics evaluation.

The input variables used in the machine learning study were reaction time, pH, dye and nanocatalyst concentrations. The absorbance (Abs) was used as the output/response variable for the ML algorithms, being converted to $C\ C_0^{-1}$ to obtain the degradation curve for the dye with the highest removal (%R). The dataset was obtained from data published in scientific papers available on literature (scopus.com), using the descriptors "methylene blue degradation" AND "photocatalytic degradation" AND "GC–MS" AND "degradation products" AND "visible light", according to the Boolean Logic. The dataset (file Mahmud_degradation_reaction_pathway.xlsx) was provided in GitHub (https://github.com/Applied-Nanomaterials-Research-Group/Machine-and-Deep-Learning), where 20 % of the dataset was used for testing. Preprocessing of data (descriptive analysis and normalization) was carried out using the Standard Scaler functions of the scikit-learn library, using the command MaxMinScaler for data resampling in values from 0 and 1.

2.8. Phytotoxicity tests

To evaluate possible phytotoxic action on seeds using Nb_2O_5-NPs, phytotoxicity tests were performed using 10 seeds of *Beta vulgaris* L. and *Brassica oleracea* grown in a receptacle containing germination paper (Germitest®) at different concentrations of 12.5, 25, 50, and 100 mg L^{-1} for 240 h at controlled temperature and humidity of 25 ± 2 °C and 65 %, respectively. In this sense, the samples were evaluated for root growth measured with a digital caliper (Mitutoyo®) and compared with the negative control (NC) that contained water and seeds [20]. Moreover, the germination index (GI) was determined by the Eq. (11).

$$GI\ (\%) = \frac{\text{Seed germination*Shoot lenght of treated water}}{\text{Seed germination*Shoot lenght of water}} * 100 \quad (11)$$

3. Results and discussion

3.1. Characterization

Fig. 1 shows the XRD diffractogram of the Nb_2O_5-NPs, where were identified the peaks associated to the pseudohexagonal of niobium oxide (Nb_2O_5) phase at $2\theta = 22.72°$ (001), 28.60° (100), 36.75° (101), 46.22° (002), 50.63° (110) and 55.29° (102) (JCPDS number 28–0317). The crystallite size of the Nb_2O_5-NPs was 21.6 ± 8.1 nm, confirming the effectiveness of the green synthesis process of nanostructured systems.

Fig. 2 informs the result of the 11 points assay, where the Nb_2O_5-NPs showed zero charge point (pH_{ZCP}) at pH 6.77, suggesting that the nanocatalyst will be protonated (positive surface charge) at pH < 6.77, and deprotonated (negative surface charge) at pH > 6.77. Thus. At pH of the assay (pH 7), the electrostatic interactions (attraction) between the cationic dyes molecules (MB, GV, Rh6G and RhB) and the Nb_2O_5-NPs surface were favored, hence, enhanced the photocatalytic degradation of the organic pollutant [21].

Table 2 presents the textural properties of the Nb_2O_5-NPs evaluated by the N_2 porosimetry and zeta potential (ZP).

According to Table 2, the Nb_2O_5-NPs nanocatalyst showed a surface area of $S_{BET} = 171\ m^2\ g^{-1}$ and a pore volume of $Vp = 0.3\ cm^3\ g^{-1}$. The particle diameter (D_p) of nanocatalysts directly influences their photocatalytic activity, mainly due to the relationship with surface area, charge recombination and electronic properties [22]. Smaller particles increase the specific surface area, offering more active sites for the

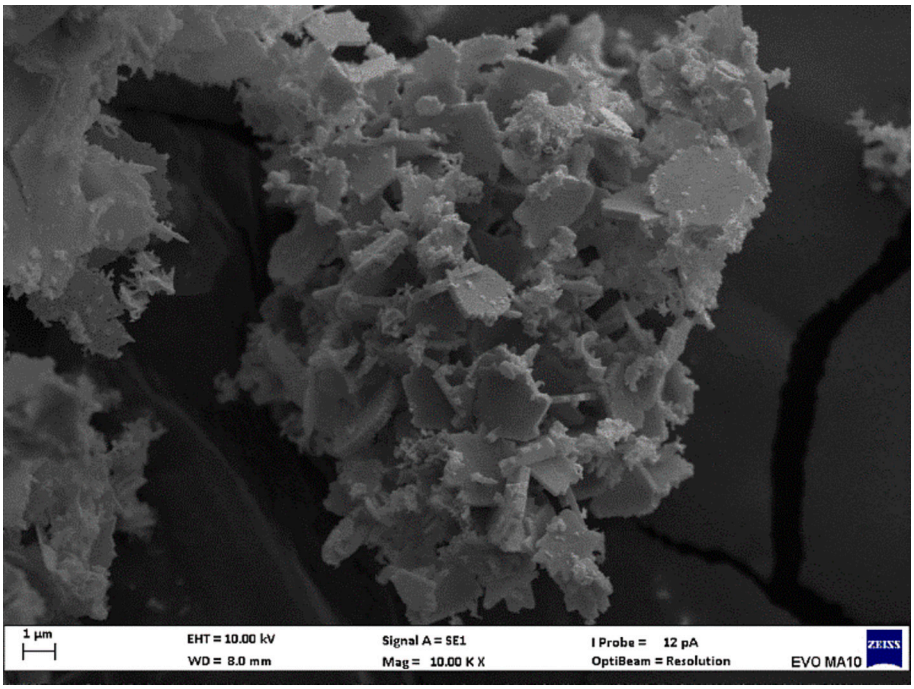

Fig. 3. Micrography of the Nb_2O_5-NPs synthesized.

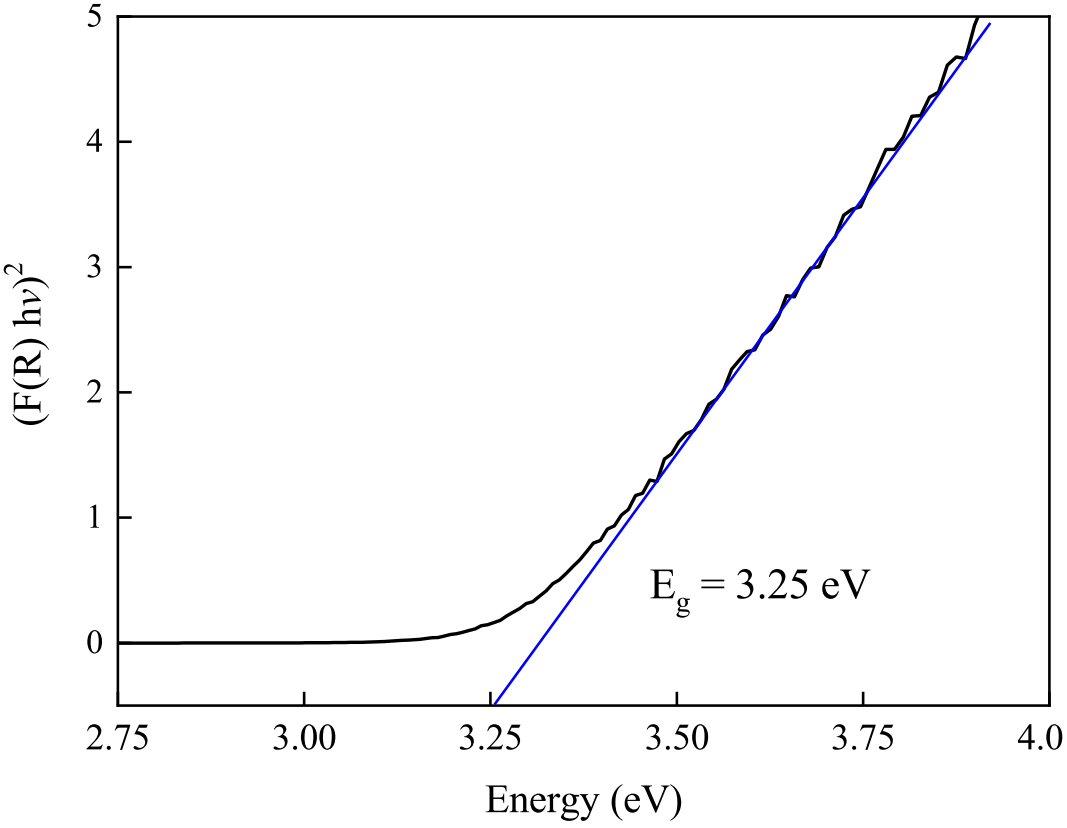

Fig. 4. Band gap energy (E_g) evaluated for Nb_2O_5-NPs from *C. illinoinensis* extract.

reaction and favoring the adsorption of reagents [23]. In addition, the reduction in size reduces the distance that the charge carriers (electrons and gaps) need to travel to the surface, reducing recombination and increasing the efficiency of the process [24]. However, smaller particles can generate aggregation and structural defects that hinder photocatalysis [25].

In parallel, another factor is the band gap, which can increase due to quantum confinement in small-size materials, improving ultraviolet light absorption but limiting absorption in the visible spectrum [26]. Thus, there is an ideal particle size that balances surface area, efficient

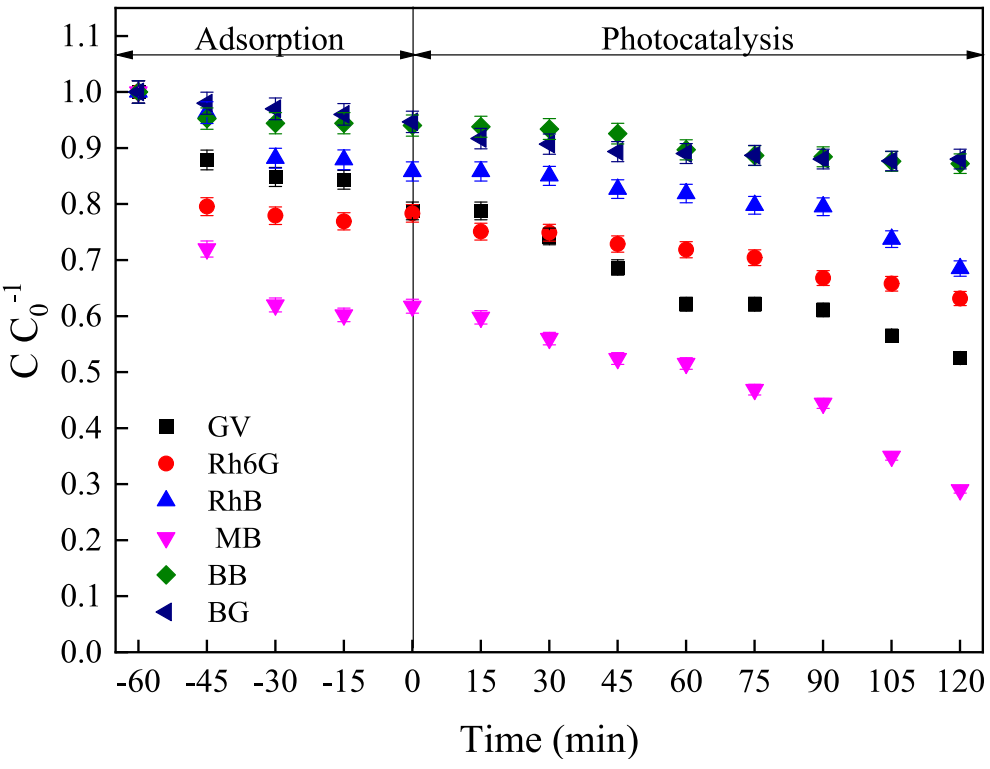

(a)

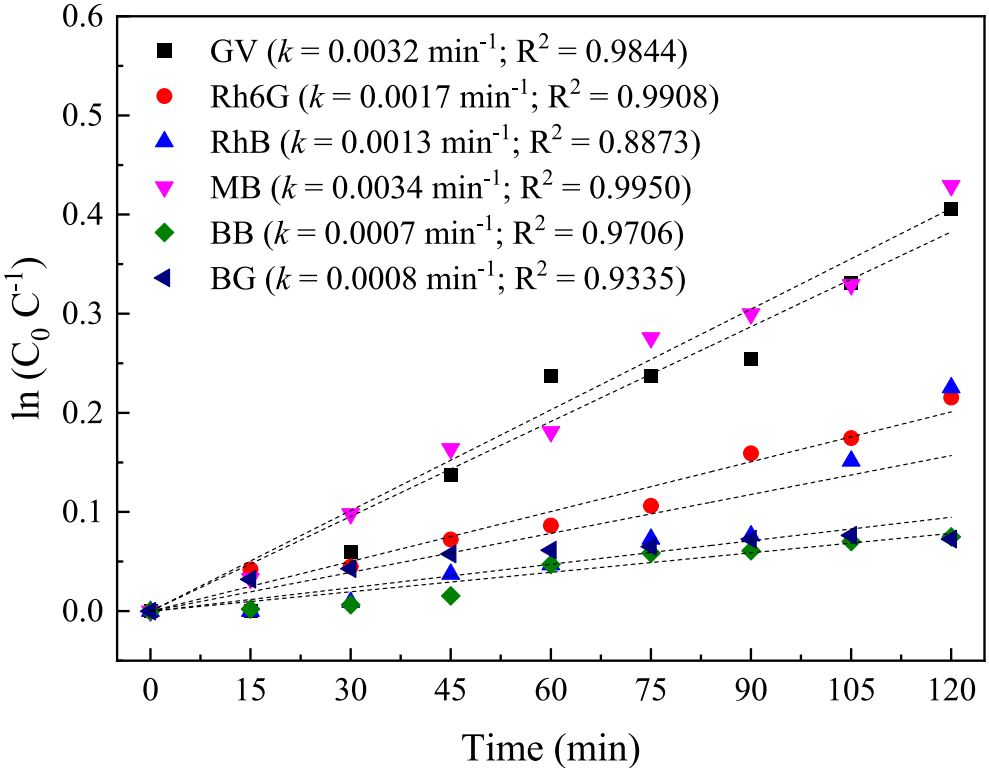

(b)

Fig. 5. (a) Photocatalytic activity of Nb_2O_5-NPs for photodegradation of organic dyes and (b) Langmuir-Hinshelwood curve fitting for dyes photodegradation under visible radiation.

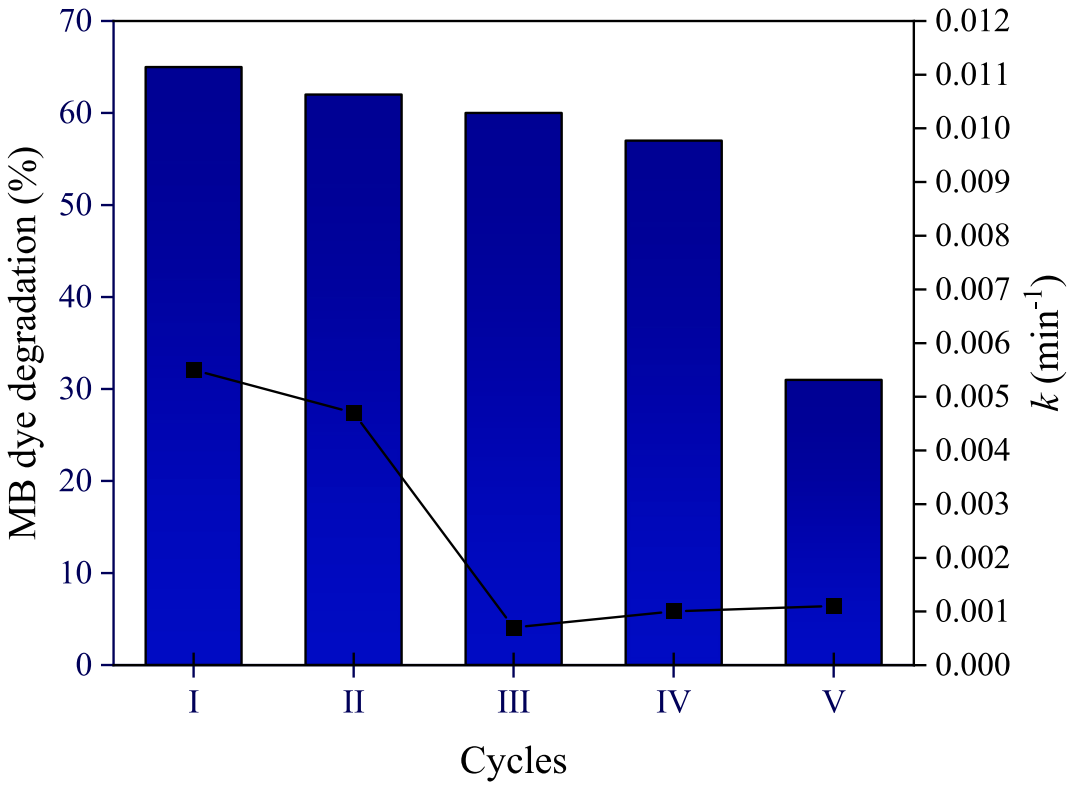

Fig. 6. Reuse of the Nb_2O_5-NPs nanocatalyst in several cycles of heterogeneous photocatalysis.

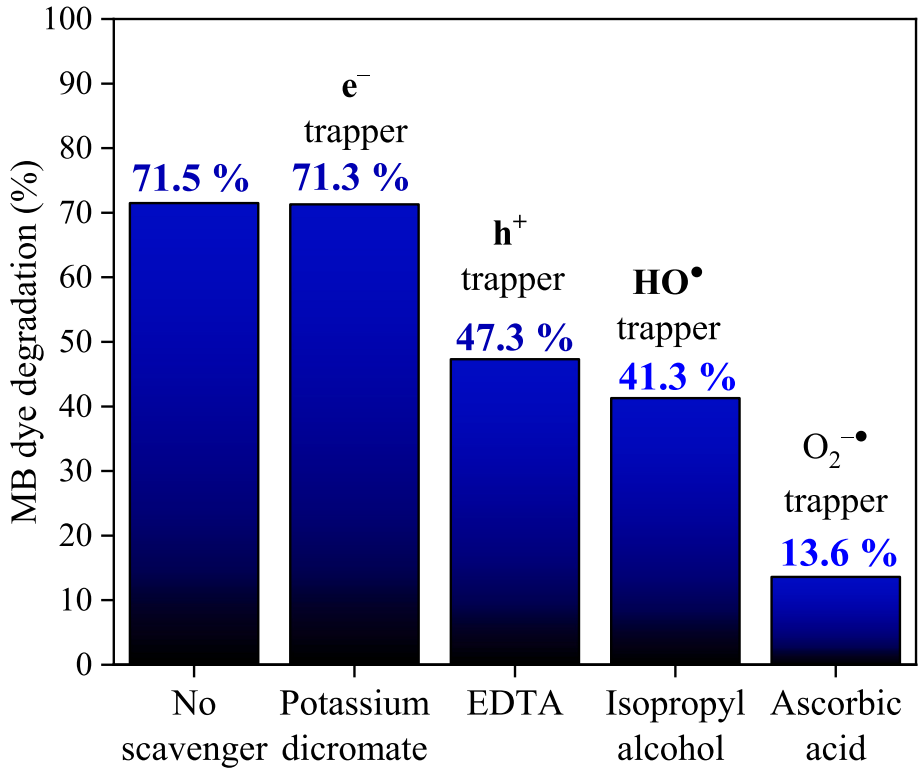

Fig. 7. Effect of the scavengers in the MB dye catalytic photodegradation.

charge transport and light absorption, maximizing photocatalytic efficiency.

Additionally, Nb_2O_5-NPs showed ZP = −28.2 ± 0.9 mV, suggesting that the nanomaterial has physicochemical stability when dispersed in an aqueous medium [27]. High ZP values prevent agglomeration, maintaining the available active surface area and increasing photocatalytic efficiency, whereas values close to zero lead to agglomeration, reducing activity [28]. In addition, ZP affects the adsorption of charged

Table 3
Performance of the algorithms tested for MB photodegradation reaction pathway.

Algorithm	$R^2_{training}$	R^2_{test}	$RMSE_{training}$	$RMSE_{test}$
DT	0.9975	0.9945	0.0059	0.0094
RF	0.9769	0.9076	0.0131	0.0519
XGBoost	0.2662	0.2792	0.1714	0.2153
RNN-LSTM	0.4419	0.4825	0.2184	0.3307

species, influencing the interaction between the catalyst and reactant molecules [29]. Fig. 3 shows the morphology of the Nb_2O_5-NPs.

According to Fig. 3, agglomerated Nb_2O_5-NPs nanoparticles with irregular morphology (plates) and heterogeneous particle sizes were identified. Fig. 4 presents the band gap energy, where Nb_2O_5-NPs showed optical activity ($E_g = 3.25$ eV), indicating photocatalytic activity of the synthesized nanocatalyst. This value of band gap energy is comparable to other nanocatalysts reported in the literature, such as s TiO_2-NPs (Eg ≈ 3.2 eV), ZnO-NPs (Eg ≈ 3.3 eV), and $BiVO_4$ (Eg ≈ 2.4–3.4 eV), which have been demonstrating efficient photocatalytic activity under UV or visible irradiation [30].

3.2. Photocatalytic degradation of organic dyes

The photocatalytic activity of the Nb_2O_5-NPs against organic dyes degradation and the curve fitting of experimental data to the Langmuir-Hinshelwood model are presented in Figs. 5(a) and 5(b), respectively.

According to Fig. 5(a), dye photodegradation varied from 7.02 % to 67 % after 120 min. The Nb_2O_5-NPs showed higher photocatalytic activity for MB dye, probably due to its lower molecular weight than others organic dyes [31], reporting near 70 % photodegradation. The adjustment of the experimental data to the Langmuir-Hinshelwood model presented in Fig. 5(b) reported values from 0.0007 min^{-1} (BB dye) to 0.0034 min^{-1} (for MB dye) for the kinetic rate constant. Moreover, the Langmuir-Hinshelwood model represented a good fit for the experimental data, showing the determination coefficient (R^2) varying from 0.89 to 0.99, suggesting that degradation reactions followed a pseudo-first-order reaction [32]. Furthermore, according to experimental observations, it was possible to observe that the increase in the molecular weight reduced the photodegradation of the dye under visible irradiation, as well as the reduction in the kinetic rate constant. This could be explained by the fact that the mass diffusion coefficient is influenced by the molecular weight of the target molecule [33]. Thus, dyes with lower molecular weights (MB and GV) presented higher removals due to the lower molecular weights compared to the other dyes (Rh 6G, RhB, BB and BG). Based on that, the photocatalytic degradation of MB dye was further investigated in terms of the reuse of the nanocatalyst, scavengers effect and main degradation products, which is discussed in the following sections.

3.3. Reuse of the nanocatalyst

Fig. 6 reports the effect of the reuse of the Nb_2O_5-NPs nanocatalyst, where it was observed that the Nb_2O_5-NPs nanocatalyst degraded around 65 % of the methylene blue dye in the first cycle, maintaining around 89.7–95.6 % of its photocatalytic activity up to 4 cycles of heterogeneous photocatalysis. After the fourth cycle, the photocatalytic activity and kinetic rate constant decreased considerably, probably due to the occupancy of active sites of the nanocatalyst with the byproducts of the dye molecules and water [34]. This result is similar to reuse study reported in the literature, in which the photocatalytic activity of niobium-based nanocatalyst for MB under ultraviolet was maintained up to four cycles [35].

3.4. Scavengers effect

Fig. 7 shows the results of the electron trappers, which were used to investigate the reactive species involved in the MB dye photocatalytic degradation, where electron (e-) generated from the activation of the photocatalyst showed no effect on the MB dye degradation, once the photocatalytic assay reported no difference in the degradation percentage (~71 %). On the contrary, EDTA, isopropyl alcohol, and

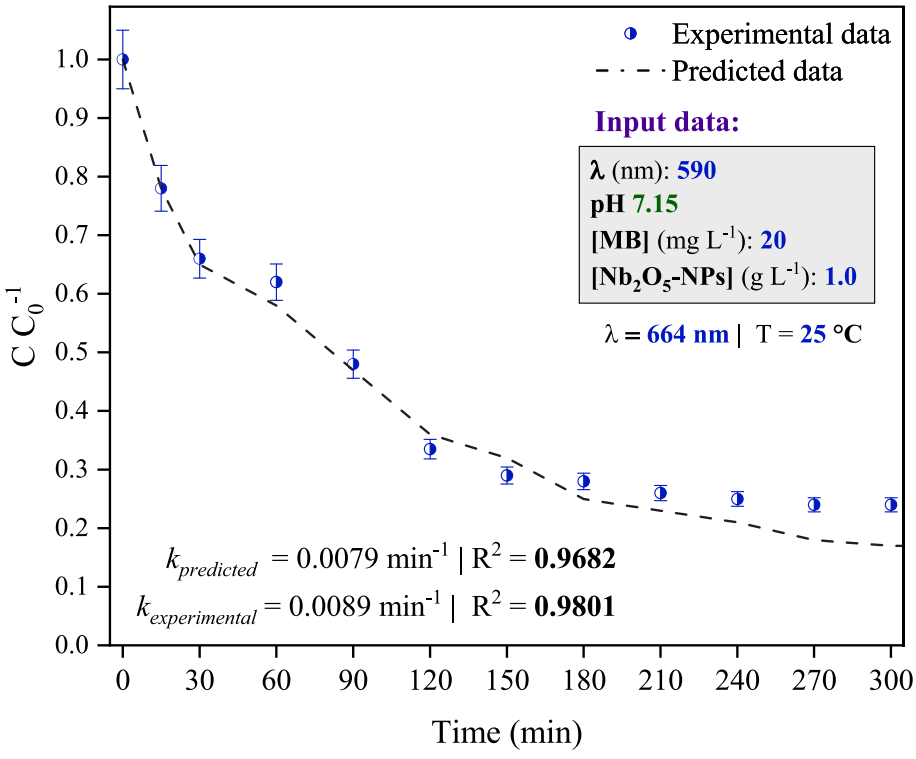

Fig. 8. Degradation reaction progress for MB dye predicted by the DT algorithm.

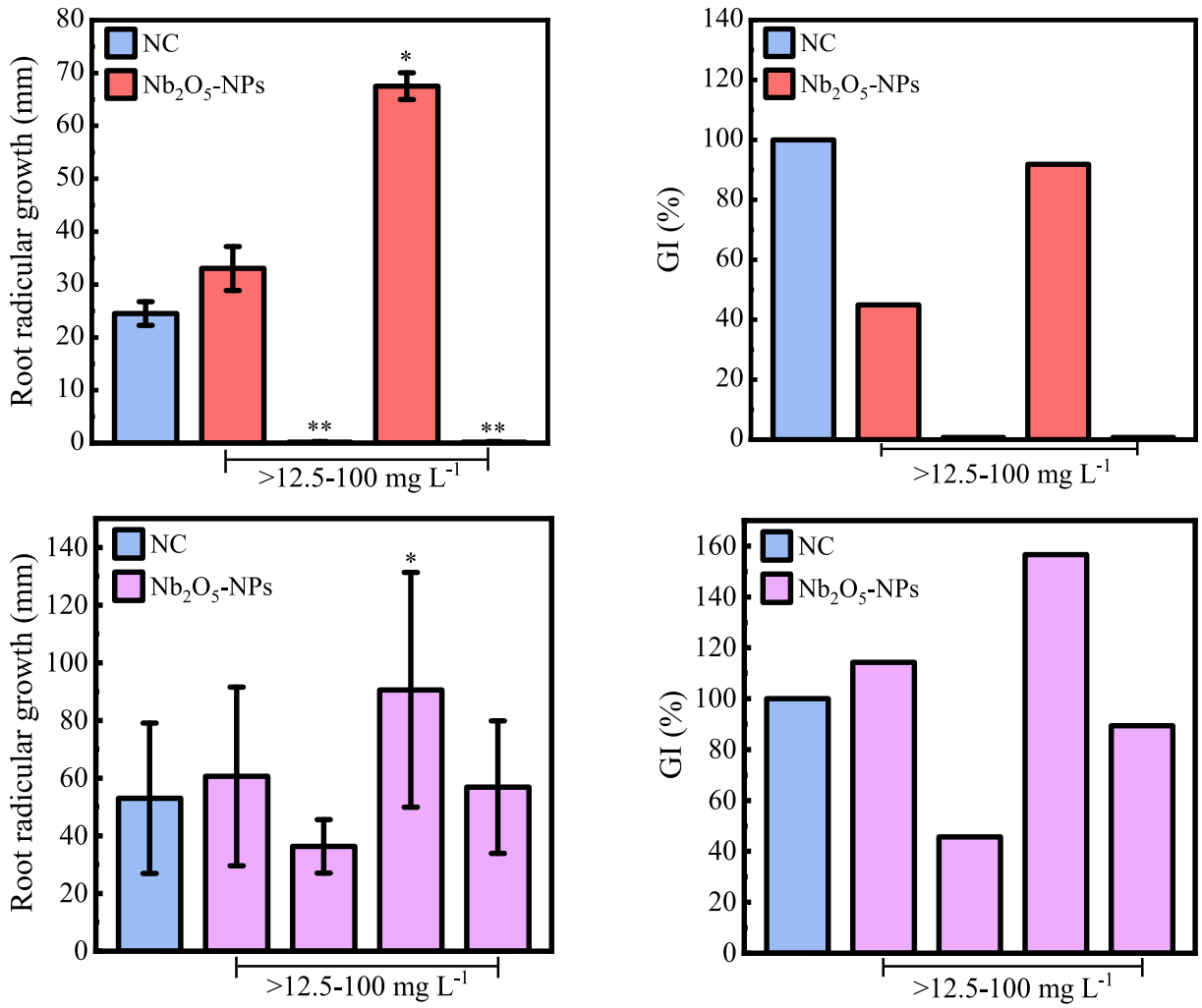

Fig. 9. (a) Radicular root growth of *Beta vulgaris L.*; (b) GI of *Beta vulgaris* L.; (c) Radicular root growth of *Brassica oleracea*; and (d) GI of *Brassica oleracea* of the Nb_2O_5-NPs. Statistical difference (one-way ANOVA) of $p < 0.033$*, $p < 0.002$** and $p < 0.001$***.

ascorbic acid lowered the MB dye degradation percentage, suggesting the presence of hole (h^+), hydroxyl radicals ($HO^{\bullet}$) and superoxide ($O_2^{\bullet}$) in the mechanism of the MB photocatalytic degradation. This result is compatible with the reports found in the literature, in which these reactive species greatly affected the dye degradation [36]. Based on this, the following section proposes a reaction pathway for MB degradation under visible radiation.

3.5. Degradation progress

Based on kinetic and degradation results, the organic dye with the highest degradation percentage and apparent rate of the pseudo first-order reaction was selected as the target molecule for the machine learning. Thus, four machine learning algorithms (Table 3) were used to investigate the photodegradation of MB dye ($k = 0.0034$ min^{-1} and 71.5 % degradation) under visible radiation.

According to Table 3, the DT algorithm showed the best performance among the ML algorithms since higher R^2 for training and test ($R^2_{training} = 0.9975$ / $R^2_{test} = 0.9945$) and lowest RMSE values ($RMSE_{training} = 0.0059$ / $RMSE_{test} = 0.0094$) were reported. Thus, DT was used to predict the degradation curve for MB dye photodegradation. Thus, Fig. 8 shows the reaction progress ($C\ C_0^{-1}$ *versus* time) for the MB dye degradation.

According to Fig. 8, the degradation of MB dye predicted by the DT algorithm was very close to the experimental value reported after 120 min (~67 % removal), with slightly higher dye degradation, reaching a *plateau* (76 % removal) after 240 min. The high determination coefficients ($R^2 = 0.9682$ for predicted and $R^2 = 0.9801$ for experimental data) demonstrate that the pseudo first-order kinetic model was a good fit of the data. Thus, the experimental and predicted pseudo first-order kinetic constant, reported for MB dye degradation, were $k_{expiremental} = 0.0089$ min^{-1} and $k_{predicted} = 0.0079$ min^{-1}, respectively.

This trend agreed with experimental reports described in the literature, where pseudo-first-order kinetics have been widely reported for MB degradation using various photocatalysts, such as CeO_2-NPs and ZnO-NPs, with comparable removal efficiencies and kinetic constants [37,38]. Moreover, the removal percentage reported in this work was close to values found in the literature in which UV radiation and ZnO-NPs were used, achieving 80 % removal of MB (20 mg L^{-1}) after 200 min [39].

3.6. Phytotoxicity of Nb_2O_5-NPs

The seed germination and growth capacity of *Beta vulgaris* L. and *Brassica oleracea* seeds are shown in Fig. 9.

According to Fig. 9(a), in the 25 and 100 mg L^{-1} (Nb_2O_5-NPs), no growth was observed for the *Beta vulgaris* L. seed, indicating high phytotoxicity for these seeds in these concentrations. Moreover, it was confirmed by the index germination in these concentrations, reporting GI < 50 % in both cases (Fig. 9b). The GI index is commonly used to

address the phytotoxicity high in the following manner: high phytotoxicity (GI < 50 %), moderate phytotoxicity (50 % < GI < 80 %) and no phytotoxicity (GI > 80 %), respectively [40]. Moreover, high phytotoxicity is observed for *Beta vulgaris* L. seed at [Nb_2O_5-NPs] = 12.5 mg L^{-1}. Thus, Nb_2O_5-NPs can be used to support plant growth (*Beta vulgaris L.* seed) only in the 50 mg L^{-1}.

As can be seen in Fig. 9(c), no significant root growth of *Brassica oleracea* was observed for all Nb_2O_5-NPs concentrations (except for the concentration of 50 mg L^{-1}). Nevertheless, an increase in root growth was observed in the 25 mg L^{-1}. Moreover, Fig. 9(d) reported a moderate phytotoxicity (50 % < GI < 80 %) for the *Brassica oleracea* seeds at [Nb_2O_5-NPs] = 25 mg L^{-1} and no phytotoxicity (GI > 80 %) in the other concentrations. Thus, it indicates that Nb_2O_5-NPs can be used as a nutrient in the *Brassica oleracea* seed and support root growth and plant development [41].

Nanoparticles-related seed root growth factors are associated with specific seed properties and types, for example, particle size, surface area, surface charge, particle agglomeration, and general seed characteristics such as maturation time, water absorption, porosity, and required micronutrients [42,43]. It is worth noting that the niobium element is not an essential element for plant growth, since its accumulation results in phytotoxic [44]. Thus, in low concentrations (12.5 mg L^{-1}) it can be used for seed root growth and catalysts.

4. Conclusion

The synthesis and characterization of green Nb_2O_5-NPs from *Carya illinoinensis* extract was proposed in this work and demonstrated effective photodegradation of methylene blue dye under visible light, achieving 71.5 % removal efficiency with a rate constant *(k)* of 0.0034 min^{-1}. The nanocatalyst exhibited favorable structural and textural properties, including high surface area and stability. According to phytotoxicity studies, Nb_2O_5-NPs showed high phytotoxicity for *Beta vulgaris L* seeds (except at 50 mg L^{-1}), and no phytotoxicity for *Brassica oleracea* seeds, in all concentration ranges tested (12.5–100 mg L^{-1}). Machine learning, specifically the DT algorithm, proved to be a powerful tool for predicting the degradation reaction progress for MB dye under visible radiation after 300 min, achieving 75 % day removal. Therefore, this study highlights the importance of integrating machine learning models into catalytic research, offering valuable insights for optimizing reaction conditions and guiding scalable photodegradation processes.

CRediT authorship contribution statement

Hanna Abdalrahman Mahmud: Writing – review & editing, Writing – original draft, Validation, Investigation, Formal analysis, Data curation, Conceptualization. **Leandro Rodrigues Oviedo:** Writing – review & editing, Writing – original draft, Validation, Methodology, Investigation, Formal analysis, Data curation. **Maurício Dalla Costa Rodrigues da Silva:** Writing – review & editing, Methodology, Formal analysis, Data curation. **Cristiane dos Santos:** Writing – review & editing, Formal analysis. **Giovani Pavoski:** Writing – review & editing, Formal analysis. **Jorge Alberto Soares Tenório:** Writing – review & editing, Formal analysis. **Denise Crocce Romano Espinosa:** Writing – review & editing, Formal analysis. **William Leonardo da Silva:** Writing – review & editing, Writing – original draft, Validation, Project administration, Investigation, Funding acquisition, Formal analysis, Data curation, Conceptualization.

Declaration of competing interest

The authors declare that they have no known competing financial interests or personal relationships that could have appeared to influence the work reported in this paper.

Acknowledgments

The authors would like to thank the Franciscan University and University of Sao Paulo (LAREX - Laboratory of Recycling, Waste Treatment and Extraction) for the support and investment in the project. This study was financed by the Conselho Nacional de Desenvolvimento Científico e Tecnológico - Brazil (CNPq/MCTI/FNDCT n° 23/2022) - InovaNióbio (n° 408422/2022-0).

Appendix A. Supplementary data

Supplementary data to this article can be found online at https://doi.org/10.1016/j.jphotochem.2025.116585.

Data availability

The data that support the findings of this study are available on request from the corresponding author. More information about the results of the machine learning study is available at the following link: https://github.com/Applied-Nanomaterials-Research-Group/Machine-and-Deep-Learning

References

[1] D.A. Yaseen, M. Scholz, Textile dye wastewater characteristics and constituents of synthetic effluents: a critical review, Int. J. Environ. Sci. Technol. 16 (2019) 1193–1226, https://doi.org/10.1007/s13762-018-2130-z.
[2] M. Chandhru, S. Kutti Rani, N. Vasimalai, Reductive degradation of toxic six dyes in industrial wastewater using diaminobenzoic acid capped silver nanoparticles, J. Environ. Chem. Eng. 8 (2020) 104225, https://doi.org/10.1016/j.jece.2020.104225.
[3] M. Liugė, D. Paliulis, Treatment of textile wastewater containing dyes, CONECT, Int. Sci. Conf. Environ. Clim. Technol. (2023) 162, https://doi.org/10.7250/CONECT.2023.129.
[4] H.R. Dihom, M.M. Al-Shaibani, R.M.S. Radin Mohamed, A.A. Al-Gheethi, A. Sharma, M.H. Bin Khamidun, Photocatalytic degradation of disperse azo dyes in textile wastewater using green zinc oxide nanoparticles synthesized in plant extract: a critical review, J. Water Process Eng. 47 (2022) 102705–102716, https://doi.org/10.1016/j.jwpe.2022.102705.
[5] A.I. Shah, M.U. Din Dar, R.A. Bhat, J.P. Singh, K. Singh, S.A. Bhat, Prospectives and challenges of wastewater treatment technologies to combat contaminants of emerging concerns, Ecol. Eng. 152 (2020) 105882, https://doi.org/10.1016/j.ecoleng.2020.105882.
[6] B. Kusumlata, A. Ambade, S. Kumar, Gautam, sustainable solutions: reviewing the future of textile dye contaminant removal with emerging biological treatments, Limnol. Rev. 24 (2024) 126–149, https://doi.org/10.3390/limnolrev24020007.
[7] G.A. Jamali, S.K. Devrajani, S.A. Memon, S.S. Qureshi, G. Anbuchezhiyan, N. M. Mubarak, S.Z.M. Shamshuddin, M.T.H. Siddiqui, Holistic insight mechanism of ozone-based oxidation process for wastewater treatment, Chemosphere 359 (2024) 142303, https://doi.org/10.1016/j.chemosphere.2024.142303.
[8] A.J. dos Santos, L.M.B. Batista, C.A. Martínez-Huitle, A.P. De M. Alves, S. Garcia-Segura, Niobium oxide catalysts as emerging material for textile wastewater reuse: photocatalytic Decolorization of azo dyes, Catalysts 9 (2019) 1070–1084, https://doi.org/10.3390/catal9121070.
[9] I. Rezić, Engineered nanoparticles in textiles and textile wastewaters, Compr. Anal. Chem. 59 (2012) 235–264, https://doi.org/10.1016/B978-0-444-56328-6.00007-4.
[10] C. Valencia-Balvín, S. Pérez-Walton, J. Peralta, J.M. Osorio-Guillén, A first-principles study of the electronic structure, surface stability, and band alignment of niobium pentoxide, Comput. Mater. Sci. 231 (2024) 112536, https://doi.org/10.1016/j.commatsci.2023.112536.
[11] C.L. Ücker, V. Goetzke, F.C. Riemke, M.E. Oliveira, N.L.V. Carreno, F.D.P. Morisso, M.D. Teodoro, V.R. Mastelaro, M.L. Moreira, C.W. Raubach, S.S. Cava, The photocatalytic performance of Fe inserted in Nb_2O_5 obtained by microwave-assisted hydrothermal synthesis: factorial design of experiments, J. Photochem. Photobiol. A Chem. 435 (2023) 114294, https://doi.org/10.1016/j.jphotochem.2022.114294.
[12] S. Ying, Z. Guan, P.C. Ofoegbu, P. Clubb, C. Rico, F. He, J. Hong, Green synthesis of nanoparticles: current developments and limitations, Environ. Technol. Innov. 26 (2022) 102336–102355, https://doi.org/10.1016/j.eti.2022.102336.
[13] J. Zhang, B. Zheng, C. Zhang, L. Xie, C. Fang, Calcined waste shells as a promising, eco-friendly adsorbent, antimicrobial, food preservative, and food packaging material: a mini review, J. Food Process Eng. 46 (2023) e14477–e14487, https://doi.org/10.1111/jfpe.14477.
[14] S. Caxambú, E. Biondo, E.M. Kolchinski, R.L. Padilha, A. Brandelli, V. Sant'anna, Evaluation of the antimicrobial activity of pecan nut [*Carya illinoinensis* (Wangenh) C. Koch] shell aqueous extract on minimally processed lettuce leaves, Food Sci. Technol. 36 (2016) 42–45, https://doi.org/10.1590/1678-457x.0043.

[15] L.F.W. Brum, M.D.C.R. Da Silva, C. dos Santos, G. Pavoski, D.C.R. Espinosa, W.L. da Silva, Green synthesis of niobium (V) oxide nanoparticles using pecan nutshell (*Carya illinoinensis*) and evaluation of its antioxidant activity, Catal. Today 445 (2025) 115106, https://doi.org/10.1016/j.cattod.2024.115106.
[16] K.D. Mahato, U. Kumar, Optimized machine learning techniques enable prediction of organic dyes photophysical properties: absorption wavelengths, emission wavelengths, and quantum yields, Spectrochim, Acta Part A Mol. Biomol. Spectrosc. 308 (2024) 123768, https://doi.org/10.1016/j.saa.2023.123768.
[17] N.G. Asenjo, R. Santamaría, C. Blanco, M. Granda, P. Álvarez, R. Menéndez, Correct use of the Langmuir–Hinshelwood equation for proving the absence of a synergy effect in the photocatalytic degradation of phenol on a suspended mixture of titania and activated carbon, Carbon N. Y. 55 (2013) 62–69, https://doi.org/10.1016/j.carbon.2012.12.010.
[18] X. Jia, F. Wang, X. Xu, C. Liu, L. Zhang, S. Jiao, G. Zhu, X. Wang, G. Yu, Highly efficient photocatalytic degradation of tetracycline by modifying UiO-66 via different regulation strategies, ACS Omega. 8 (2023) 27375–27385, https://doi.org/10.1021/acsomega.3c02762.
[19] L.R. Oviedo, D.M. Durzian, G.E. Montagner, Y.P.M. Ruiz, A. Galembeck, G. Pavoski, D.C.R. Espinosa, L.D. Dalla Nora, W.L. da Silva, Supported heterogeneous catalyst of the copper oxide nanoparticles and nanozeolite for binary dyes mixture degradation: machine learning and experimental design, J. Mol. Liq. 402 (2024) 124763, https://doi.org/10.1016/j.molliq.2024.124763.
[20] M. Kumar, M.N.M. Ansari, I. Boukhris, M.S. Al-Buriahi, Z.A. Alrowaili, N. Alfryyan, P. Thomas, R. Vaish, Sonophotocatalytic dye degradation using rGO-$BiVO_4$ composites, Glob. Challenges. 6 (2022), https://doi.org/10.1002/gch2.202100132.
[21] S. Muzammal, A. Ahmad, M. Sheraz, J. Kim, S. Ali, M.B. Hanif, I. Hussain, S. Pandiaraj, A. Alodhayb, M.S. Javed, H.A.Z. Al-bonsrulah, M. Motola, Polymer-supported nanomaterials for photodegradation: unraveling the methylene blue menace, Energy Convers. Manag. X. 22 (2024) 100547, https://doi.org/10.1016/j.ecmx.2024.100547.
[22] K. Yoshida, Role of nanoparticle size in the photocatalytic degradation of pollutants, J. Chemother. 3 (2024) 12–20, https://doi.org/10.47672/jchem.2405.
[23] B. Kirchhoff, C. Jung, D. Gaissmaier, L. Braunwarth, D. Fantauzzi, T. Jacob, In silico characterization of nanoparticles, Phys. Chem. Chem. Phys. 25 (2023) 13228–13243, https://doi.org/10.1039/D3CP01073B.
[24] H.-R. Tseng, S.-C. Hsu, S.-L. Lin, Y.-H. Chen, C.-C. Lin, Surface recombination dependent performance of a nano-scale p-n junction solar cell, in: IEEE 40th Photovolt. Spec. Conf. 2014, IEEE, 2014, pp. 1106–1109, https://doi.org/10.1109/PVSC.2014.6925109.
[25] J. Gupta, P.A. Hassan, K.C. Barick, Defects in Nanomaterials for Visible Light Photocatalysis, in: Nanostructured Mater. Visible Light Photocatal., Elsevier, in, 2022, pp. 319–350, https://doi.org/10.1016/B978-0-12-823018-3.00002-6.
[26] H. Meddeb, M. Gotz-Kohler, N. Osterthun, O. Sergeev, K. Gehrke, M. Vehse, C. Agert, Investigation of quantum size effects on the optical absorption in ultrathin single quantum well solar cell embedded as a Nanophotonic resonator, IEEE J. Photovoltaics. 12 (2022) 760–770, https://doi.org/10.1109/JPHOTOV.2022.3150726.
[27] A. Carone, S. Emilsson, P. Mariani, A. Désert, S. Parola, Gold nanoparticle shape dependence of colloidal stability domains, Nanoscale Adv. 5 (2023) 2017–2026, https://doi.org/10.1039/D2NA00809B.
[28] Y. Bai, H. Huang, C. Wang, R. Long, Y. Xiong, Engineering the surface charge states of nanostructures for enhanced catalytic performance, Mater. Chem. Front. 1 (2017) 1951–1964, https://doi.org/10.1039/C7QM00020K.
[29] Y. Shi, Z. Wang, Y. Song, J.C. Yu, L. Wu, Designing efficient 2D Photocatalysts through coordination activation mediated surface engineering, ChemCatChem 16 (2024), https://doi.org/10.1002/cctc.202401037.
[30] A.A. Mohd Raub, R. Bahru, M.A. Mohamed, R. Latif, M.A.S. Mohammad Haniff, K. Simarani, J. Yunas, Photocatalytic activity enhancement of nanostructured metal-oxides photocatalyst: a review, Nanotechnology 35 (2024) 242004, https://doi.org/10.1088/1361-6528/ad33e8.
[31] N.A.A. Suhaimi, N.N.M. Shahri, J.H. Samat, E. Kusrini, J.W. Lim, J. Hobley, A. Usman, Domination of methylene blue over rhodamine B during simultaneous photocatalytic degradation by TiO2 nanoparticles in an aqueous binary solution under UV irradiation, React. Kinet. Mech. Catal. 135 (2022) 511–527, https://doi.org/10.1007/s11144-021-02098-2.
[32] H.D. Tran, D.Q. Nguyen, P.T. Do, U.N.P. Tran, Kinetics of photocatalytic degradation of organic compounds: a mini-review and new approach, RSC Adv. 13 (2023) 16915–16925, https://doi.org/10.1039/D3RA01970E.
[33] M. Shabil Sha, H. Anwar, F.N. Musthafa, H. Al-Lohedan, S. Alfarwati, J. R. Rajabathar, J. Khalid Alahmad, J.-J. Cabibihan, M. Karnan, K. Kumar Sadasivuni, Photocatalytic degradation of organic dyes using reduced graphene oxide (rGO), Sci. Rep. 14 (2024) 3608, https://doi.org/10.1038/s41598-024-53626-8.
[34] G. Salehi, M. Bagherzadeh, R. Abazari, M. Hajilo, D. Taherinia, Visible light-driven photocatalytic degradation of methylene blue dye using a highly efficient mg–Al LDH@g-C_3N_4@Ag_3PO_4 nanocomposite, ACS Omega 9 (2024) 4581–4593, https://doi.org/10.1021/acsomega.3c07326.
[35] E. De P. Ferreira, S.R.F.L. Ribeiro, T.S.E. Sousa, V.L. Cardoso, M.H.M. Reis, Surface decoration of Nb_2O_5 hollow fibers by graphene oxide for enhanced photocatalytic degradation of methylene blue, J. Am. Ceram. Soc. 108 (2025), https://doi.org/10.1111/jace.20176.
[36] V. Arumugaperumal, S. K, Solar light driven photocatalytic degradation of methylene blue dye over cu doped α-MnO_2 nanoparticles, Chem. Phys. Impact. 8 (2024) 100434, https://doi.org/10.1016/j.chphi.2023.100434.
[37] S. Li, P. Zhou, W. Zhang, S. Chen, H. Peng, Effective photocatalytic decolorization of methylene blue utilizing ZnO/rectorite nanocomposite under simulated solar irradiation, J. Alloys Compd. 616 (2014) 227–234, https://doi.org/10.1016/j.jallcom.2014.07.102.
[38] Z. Kalaycioglu, B.O. Uysal, O. Peckcan, F.B. Erim, Efficient photocatalytic degradation of methylene blue dye from aqueous solution with cerium oxide nanoparticles and graphene oxide-doped polyacrylamide, ACS Omega 8 (2023) 13004–13015, https://doi.org/10.1021/acsomega.3c00198.
[39] H. Etay, A. Kumar, O.P. Yadav, Kinetics of photocatalytic degradation of methylene blue dye in aqueous medium using ZnO nanoparticles under UV radiation, J. Anal. Pharm. Res. 12 (2023) 32–37.
[40] M.A.M. Castro, R.A. Oliveira, J.M.P. Silva, M.D. Teodoro, U.C. Silva, M.R.D. Bomio, F.V. Motta, Solar-enhanced photodegradation of dye and drug mixture and evaluation of phytotoxicity on seed germination and growth by an eggshell HAp/Nb_2O_5 heterostructure, Ceram. Int. 50 (2024) 19124–19136, https://doi.org/10.1016/j.ceramint.2024.03.011.
[41] H. Zeghioud, N. Khellaf, A. Amrane, H. Djelal, M. Bouhelassa, A.A. Assadi, S. Rtimi, Combining photocatalytic process and biological treatment for reactive green 12 degradation: optimization, mineralization, and phytotoxicity with seed germination, Environ. Sci. Pollut. Res. 28 (2021) 12490–12499, https://doi.org/10.1007/s11356-020-11282-1.
[42] M. Liu, S. Feng, Y. Ma, C. Xie, X. He, Y. Ding, J. Zhang, W. Luo, L. Zheng, D. Chen, F. Yang, Z. Chai, Y. Zhao, Z. Zhang, Influence of surface charge on the Phytotoxicity, transformation, and translocation of CeO_2 nanoparticles in cucumber plants, ACS Appl. Mater. Interfaces 11 (2019) 16905–16913, https://doi.org/10.1021/acsami.9b01627.
[43] Z. Li, W. Yan, Y. Li, Y. Xiao, Y. Shi, X. Zhang, J. Lei, K. Min, Y. Pan, X. Chen, Q. Liu, G. Jiang, Particle size determines the Phytotoxicity of ZnO nanoparticles in Rice (*Oryza sativa* L.) revealed by spatial imaging techniques, Environ. Sci. Technol. 57 (2023) 13356–13365, https://doi.org/10.1021/acs.est.3c03821.
[44] A. Priac, P.-M. Badot, G. Crini, Treated wastewater phytotoxicity assessment using Lactuca sativa: focus on germination and root elongation test parameters, Comptes Rendus. Biol. 340 (2017) 188–194, https://doi.org/10.1016/j.crvi.2017.01.002.